Photoacoustics 18 (2020) 100166

Contents lists available at ScienceDirect

Photoacoustics

journal homepage: www.elsevier.com/locate/pacs

Prussian blue nanocubes as a multimodal contrast agent for image-guided stem cell therapy of the spinal cord

Kelsey P. Kubelick[a,b], Stanislav Y. Emelianov[a,b,*]

[a] Wallace H. Coulter Department of Biomedical Engineering, Georgia Institute of Technology and Emory University School of Medicine, 313 Ferst Dr NW, Atlanta, GA, 30332, USA

[b] School of Electrical and Computer Engineering, Georgia Institute of Technology, 777 Atlantic Drive, Atlanta, GA, 30332, USA

ARTICLE INFO

Keywords:
Photoacoustic imaging
Ultrasound
Magnetic resonance imaging
Multimodal imaging
Spinal cord
Stem cells
Nanoparticles

ABSTRACT

Translation of stem cell therapies to treat injuries and diseases of the spinal cord is hindered by lack of real-time monitoring techniques to guide regenerative therapies intra- and postoperatively. Thus, we developed an ultrasound (US), photoacoustic (PA), and magnetic resonance (MR) imaging approach augmented with Prussian blue nanocubes (PBNCs) to guide stem cell injections intraoperatively and monitor stem cell therapies in the spinal cord postoperatively. Per the clinical procedure, a multi-level laminectomy was performed in rats *ex vivo*, and PBNC-labeled stem cells were injected directly into the spinal cord while US/PA images were acquired. US/PA/MR images were also acquired post-surgery. Several features of the imaging approach were demonstrated including detection of low stem cell concentrations, real-time needle guidance and feedback on stem cell delivery, and good agreement between US/PA/MR images. These benefits span intra- and postoperative environments to support future development of this imaging tool.

1. Introduction

Regenerative medicine holds great promise to offer novel treatment methods for injuries and neurodegenerative diseases of the spinal cord. Stem cell therapy has received substantial interest, but has not yet reached its clinical potential [1–5]. Development and translation of stem cell therapies for the spinal cord is hindered by several factors including lack of: 1) real-time guidance of the stem cell injection; 2) noninvasive, longitudinal monitoring techniques to assess treatment progression and improve understanding of stem cell behavior; and 3) functional stem cell monitoring [6–8]. Thus, development of imaging tools to guide stem cell therapy in the spinal cord throughout the course of treatment is a critical step to expedite development and clinical translation of these regenerative therapies.

Others have recognized this need and substantial effort has been spent developing magnetic resonance imaging (MRI) tools using superparamagnetic iron oxide nanoparticles (SPIONs) or other types of magnetic beads to detect stem cells in the spinal cord [9–13]. MRI is the gold standard for spinal cord imaging; however, it still has disadvantages, including high cost, slow acquisition time, large foot print, lack of portability, and operating room (OR) incompatibility [14–16]. For these reasons, the use of MRI to guide stem cell therapies throughout the entire course of treatment is challenging. Other modalities may be able to address these shortcomings to create a more versatile method for guiding stem cell therapies in the spinal cord. One option is combined ultrasound and photoacoustic (US/PA) imaging [17–21].

Ultrasound (US) signals are produced by backscattering of acoustic waves to convey anatomical information at high resolution. However, contrast is poor due to similar backscattering properties across many tissues. Photoacoustic (PA) imaging can address this challenge. In PA imaging, contrast is based on absorption of light rather than scattering of sound. By irradiating an optical absorber with a pulsed laser, thermal expansion of the surrounding tissue produces transient acoustic waves that can be detected by a traditional ultrasound transducer [19–21]. Benefits of PA imaging include high contrast, high resolution, real-time imaging, low cost, and portability to more easily facilitate intra- or postoperative imaging of stem cell therapies. Together, ultrasound provides anatomical context, and photoacoustic imaging can convey tissue function at the cellular level.

Abbreviations: AuNS, gold nanosphere; DIUF, deionized ultra-filtered water; IACUC, Institutional Animal Care and Use Committee; LOD, limit of detection; MRI, magnetic resonance imaging; MSC, mesenchymal stem cell; OR, operating room; PA, photoacoustic; PBNC, Prussian blue nanocube; PBS, phosphate buffered saline; SPION, superparamagnetic iron oxide nanoparticle; TE, echo time; TEM, transmission electron microscopy; TR, repetition time; US, ultrasound

* Corresponding author at: School of Electrical and Computer Engineering, Georgia Institute of Technology, 777 Atlantic Drive, Atlanta, GA, 30332, USA.
E-mail address: stas@gatech.edu (S.Y. Emelianov).

https://doi.org/10.1016/j.pacs.2020.100166
Received 16 August 2019; Received in revised form 20 January 2020; Accepted 3 February 2020
Available online 10 March 2020

Stem cells must be labeled with an optical absorber to allow PA detection. A variety of exogenous contrast agents exist to address this need [17,22]. We previously explored the use of gold nanosphere (AuNS)-labeled stem cells in the spinal cord for US/PA imaging [6]. Results with AuNSs showed potential for intraoperative guidance, but extension to postoperative monitoring in the spinal cord may be hindered due to limited imaging penetration depth. A better approach may be to use a multimodal contrast agent that allows guidance of stem cell therapies with US/PA/MRI. Combined advantages of these modalities can allow real-time, intraoperative guidance and improved postoperative stem cell tracking. Furthermore, this strategy integrates more seamlessly with the current clinical practice by providing tools to be used in addition to MRI, rather than attempting to replace the standard of care.

Here, we developed a US/PA/MRI approach to facilitate intra- and postoperative guidance of stem cell therapies in the spinal cord. The key to the approach is the use of Prussian blue nanocubes (PBNCs) to label stem cells and generate multimodal contrast. Prussian blue-based nanoparticles have been investigated in other applications of PA imaging or MRI separately [23–29]. Our specific formulation of PBNCs are synthesized using a unique method, where commercially available SPIONs serve as reaction precursors [30]. The diameter of the SPION precursor ultimately dictates edge length of the resulting PBNC to enhance and tailor optical or magnetic properties for different applications [30].

Here, stem cells were labeled with PBNCs with a 200 nm edge length and injected in the spinal cord followed by US/PA and MRI as it would be performed in intraoperative and postoperative scenarios. The goal of the study was to demonstrate feasibility of US/PA/MRI augmented with PBNCs to guide stem cell therapies in the spinal cord throughout the course of treatment. Several features of the approach were highlighted, including detection of stem cells at low concentrations, real-time needle guidance and injection monitoring, feedback on stem cell delivery, and agreement between PA and MR images. Overall results motivate further development of a US/PA/MRI approach for stem cell tracking in the spinal cord to provide more complete feedback for clinicians and researchers to guide therapy.

2. Materials and methods

2.1. Nanoparticle synthesis and characterization

All reaction components were used as received and were purchased from Sigma-Aldrich, unless otherwise stated. PBNCs were produced using previously reported methods [30]. Briefly, the reactant, 5% by mass of potassium hexacyanoferrate (II) trihydrate in deionized ultrafiltered (DIUF) water, and the catalyst, 5% by volume of 37 % HCl in DIUF water, were prepared. While stirring, 60 mg of SPIONs (Ocean Nanotech) were added to 150 ml of DIUF water, followed by 7.5 ml of the reactant and 2.5 ml of the catalyst. The reaction was stirred for at least 1 h. PBNCs were dextran coated by adding 10 mg of dextran/mg of Fe. Transmission electron microscopy (TEM) (HT7700, Hitachi) was used to characterize PBNC morphology. The optical absorption spectrum of PBNCs was measured using a UV–vis spectrophotometer (Evolution 220, Thermo Fisher). Longitudinal and transverse relaxivity of the PBNCs suspended in phosphate buffered saline (PBS) was determined using a low-field 0.5 T NMR spectrometer (Maran Ultra 23, Resonance), and the average relaxation time was calculated using four scans per sample, each of which contained a different concentration of particles.

2.2. Stem cell labeling with PBNCs

Human adipose-derived mesenchymal stem cells (MSCs) (Lonza) were cultured using standard protocols in α -minimum essential medium (Corning) supplemented with 20 % fetal bovine serum (Phenix Research), 5% L-glutamine, and 1% penicillin/streptomycin (Thermo Fisher). MSCs did not exceed passage 9. Cells were incubated with particles at ~80 % confluence. Prior to 24 -h incubation with cells, PBNCs were sterilized for at least 30 min under UV light. The old cell media was aspirated and replaced with fresh media containing PBNCs at an optical density (OD) of 1–2, corresponding to roughly 26–53 μg Fe/ml. PBNC-labeled MSCs were washed with PBS, trypsinized, and centrifuged to further remove any residual PBNCs. PBNC-labeled MSCs used for *in vitro* experiments were fixed in 10 % neutral buffered formalin for 15 min. PBNC-labeled MSCs for *ex vivo* experiments were resuspended in PBS and kept on ice. PBNC-labeled MSCs were stained with eosin (VWR) to confirm PBNC uptake with bright-field microscopy.

2.3. Imaging instruments

All US/PA imaging experiments were conducted using the Vevo LAZR (FujiFilm Visualsonics, Inc.). US/PA images were acquired at a frame rate of 5 Hz using a 20 MHz ultrasound transducer integrated with fiber optic light delivery (LZ 250) and interfaced with a tunable (680 − 970 nm wavelength range) optical-parametric oscillator (OPO) laser system pumped by a Q-switched Nd:YAG laser (20 Hz laser pulse repetition frequency, 7 ns laser pulse duration).

A 7 T preclinical MRI system (Bruker PharmaScan) was used to acquire all MR images. Samples were secured in a 38 mm imaging coil. Built-in pulse sequences were used with modifications to the repetition time (TR) and echo time (TE), described in detail for each experiment, to improve nanoparticle contrast.

2.4. In vitro studies using tissue models

A tissue-mimicking phantom was used to assess US/PA and MR signal from PBNC-labeled MSCs [31]. The phantom base consisted of 8% gelatin and 0.2 % silica by mass. Cells suspended in 8% gelatin were pipetted onto the phantom base to form 40 μl inclusions (semi-spherical domes) containing PBNC-labeled MSCs at 10k, 5k, 2.5k, 1.25k, 625, 313, 156, 78, 39, 20, and 0 cells/μl. The phantom was submerged in water and imaged using US/PA and MRI.

Cross-sectional US/PA images of the inclusions were acquired at 740 nm wavelength, corresponding to the PBNC optical absorption peak determined by UV–vis spectrophotometry. Each inclusion was identified using cross-sectional ultrasound images, and the average PA signals were calculated over 20 frames to minimize the influence of laser energy fluctuations.

MR images were acquired using a multi-slice multi-echo (MSME) pulse sequence to determine T2 relaxation times starting with TR = 1955.2 ms and TE = 20 ms. TE increased by 20 ms increments for 32 steps. Due to better visualization of inclusions, coronal views were acquired and analyzed. Although different slice orientations were used for PA and MRI, slice orientation was not expected to impact results. The Bruker software was used to define a circular region of interest corresponding to the inclusion, and the average T2 relaxation time and standard deviation were calculated using the built-in parametric fit feature.

The limit of detection (LOD) for PA and MR images of cell inclusions was calculated using previously established methods [32]:

$$\mathrm{LOD} = 2\sigma_{blank} + A_{blank} + 2\sigma_{cells}$$

where σ is the standard deviation and A_{blank} is the signal amplitude for PA data or the relaxation time for MR data measured from the inclusion containing gelatin only (*i.e.* no cells). To calculate the PA limit of detection, data from all cell concentrations were included. To calculate the MR limit of detection, data from the inclusions containing 5000 cells/μl or less were included because the MR signal from inclusions containing higher cell concentrations was likely saturated, at which point the above the equation no longer holds [32].

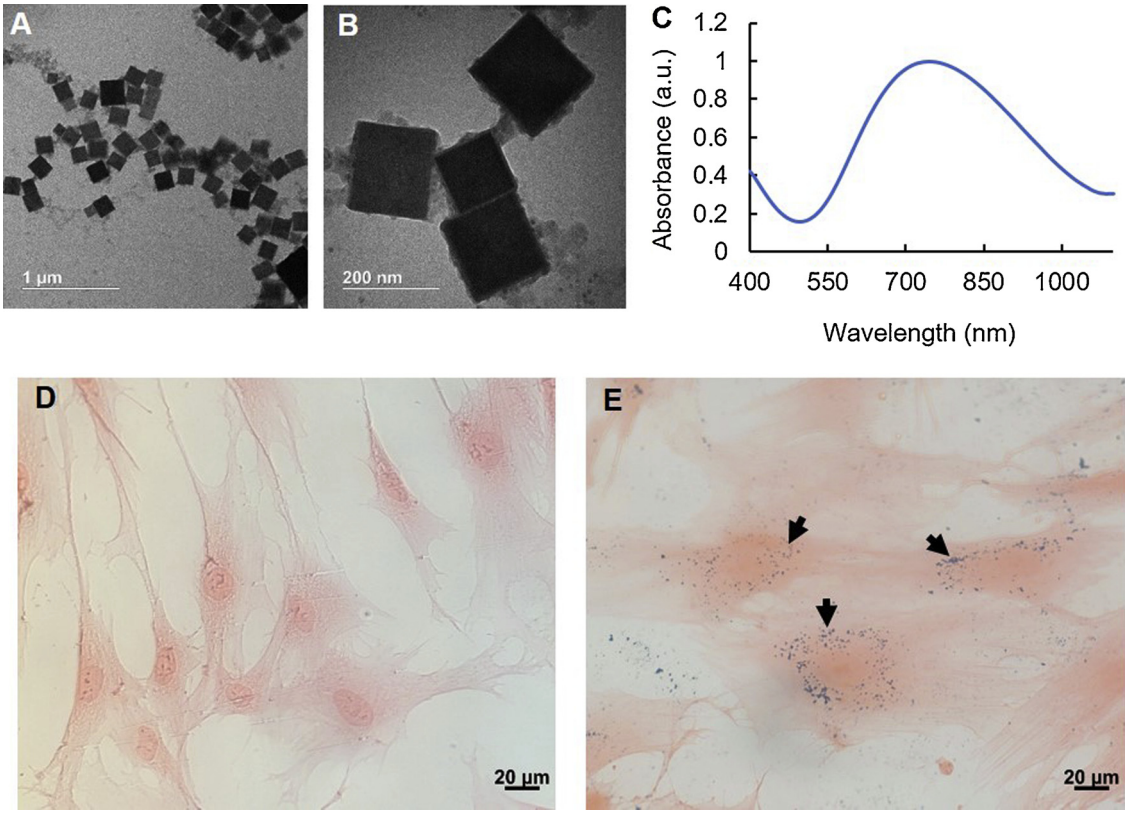

Fig. 1. Characterization of Prussian blue nanocubes (PBNCs) and labeled stem cells. (A, B) Transmission electron microscopy (TEM) of dextran-coated PBNCs with an edge length of ~200 nm. (C) Absorption spectrum of PBNCs, measured by UV–vis spectrophotometry, showed a peak optical absorption at 734 nm wavelength. Histology of eosin-stained adipose-derived mesenchymal stem cells (MSCs) confirmed successful cell labeling with PBNCs (D, E). Naïve MSCs (D) and MSCs incubated with PBNCs at 2 OD (E) at 40x magnification. PBNCs are blue in color and are indicated by black arrows. Proceeding studies were conducted with PBNCs at a concentration of 1 OD.

2.5. Spinal cord access and stem cell injection protocol

All Sprague-Dawley rat studies followed previously reported methods and were conducted according to guidelines established by the Institutional Animal Care and Use Committee (IACUC) at the Georgia Institute of Technology [6,33–35]. In brief, following euthanasia the spinal column was removed and a multi-level laminectomy was performed to expose the underlying spinal cord. Up to 5 μl of PBNC-labeled MSCs suspended in PBS at 10k cells/μl were directly injected into the spinal cord per the clinical procedure at a rate of 16 nl/sec using a 33 G syringe attached to an ultra-micropump (World Precision Instruments).

2.6. Real-time US/PA imaging during needle insertion and post-processing

During needle insertion, US/PA datasets were acquired at 740 nm wavelength and exported to MATLAB for post-processing. Reverberation artifacts extending below the needle shaft were removed by creating a mask with a width of 2x the outer diameter of the 33 G needle used for the injection, and the mask was aligned along the longitudinal axis of the needle shaft. Small gaps in the PA signal were occasionally observed along the needle shaft, and the MATLAB image processing toolbox and morphological operators, specifically image dilation followed by erosion, were used to display a continuous needle shaft.

2.7. Real-time US/PA imaging during stem cell injections and post-processing

During stem cell injections, US/PA datasets were acquired at 740 nm wavelength and exported to MATLAB for post-processing. Photoacoustic signals from the needle shaft and PBNC-labeled MSCs were segmented to better visualize the injection by partitioning PA images into a set of pixels representing: 1) the needle shaft or 2) the stem cells. For the needle shaft, reverberations artifacts were removed as described above. Any remaining PA pixels in the injection region were identified as PBNC-labeled MSCs. As a result, PBNC-labeled MSCs were primarily colored red, and the needle shaft was primarily colored blue. The average PA signal was calculated for the region containing the PBNC-labeled stem cells.

2.8. US/PA/MR imaging after stem cell injections and post-processing

Injection locations were marked with glass capillary tubes, visible in ultrasound and MRI, to assure the same injections were compared across modalities.

In post-injection studies, three-dimensional (3D) US/PA datasets were produced by attaching the transducer to a translational motorized stage and compiling two-dimensional (2D) cross-sectional images acquired at 133 μm steps and 740 nm wavelength. Volumetric US/PA datasets were acquired with and without a layer of muscle covering the spinal cord. Datasets were exported and post-processed in MATLAB.

Sagittal US/PA images were obtained from the reconstructed 3D datasets and were interpolated to display images with square pixels (~40 μm by ~40 μm). Anatomical information provided by ultrasound imaging was used to spatially distinguish PA signals from different species: 1) blood vessels/background signals on top of the spinal cord; 2) PBNC-labeled stem cells within the spinal cord. PA signals from each species were segmented to primarily color background signals blue and PBNC-labeled MSCs red. Reverberation artifacts, occasionally observed underneath the blood vessels with strong PA signals, were removed by

finding the local maximum PA signal, which corresponded to the vessel, and eliminating PA signals within a 1 mm mask width.

All MR images were captured with a layer of muscle placed on top of the spinal cord. MR images were acquired using several different pulse sequences. Images with T2-weighted contrast were obtained using the T2-Turbo RARE sequence with TR = 2500 ms and TE = 35 ms. Images with T2*-weighted contrast were obtained using the T1-FLASH sequence with TR = 310 ms and TE = 5–10 ms. Four averages were used in all pulse sequences.

Following US/PA/MR imaging, spinal cord tissue was sliced for histological analysis and imaged using bright-field microscopy (Zeiss Axio Observer).

3. Results

TEM showed that the synthesized PBNCs had an edge length of ~200 nm (Fig. 1 A, B). This was expected based on results reported previously [30]. UV–vis spectrophotometry showed a peak optical absorption of PBNCs at 734 nm (Fig. 1C). The longitudinal and transverse relaxation times of the PBNCs were 77.9 $mM^{-1}s^{-1}$ and 4.15 $mM^{-1}s^{-1}$, respectively. Bright-field photomicrographs (Fig. 1D, E) confirmed stem cell uptake of PBNCs, indicated by blue speckles co-localized with pink, eosin-stained cytoplasm.

PA imaging experiments were conducted *in vitro* using a tissue-mimicking phantom with inclusions to confirm PBNC-labeled MSCs produced PA contrast. Each dome-shaped gelatin inclusion contained PBNC-labeled MSCs at known cell concentrations (Fig. 2A). Qualitatively, ultrasound signal (top row; grayscale) and PA signal (bottom row; colorscale) decreased with decreasing cell concentration (Fig. 2A). The average PA signal was calculated for each inclusion and confirmed PA signal decreased with decreasing cell concentration (Fig. 2B). Some variations were observed in this trend, likely due to heterogeneous distribution of labeled cells at lower concentrations, and subtle changes in transducer position in different imaging frames, which impacted light fluence and ultimately PA signal amplitude. Nevertheless, calculations indicated PA imaging had a limit of detection on the order of 100 cells/μl. The representative PA spectrum of PBNC-labeled MSCs (Fig. 2C) was similar to UV–vis spectrophotometry results (Fig. 1C).

MR images were acquired for the same tissue-mimicking phantom with inclusions to confirm PBNC-labeled MSCs produced MR contrast and to compare detection limits of PA *versus* MRI. Although the T2 relaxation time generally increased as PBNC-labeled MSC concentration decreased (Fig. 3), a consistent, clear trend was not observed. Calculations indicated MRI had a limit of detection on the order of 1000 cells/μl. Although the *in vitro* study indicated PA imaging was more sensitive than MRI to lower cell concentrations, both modalities successfully detected PBNC-labeled MSCs at clinically relevant concentrations.

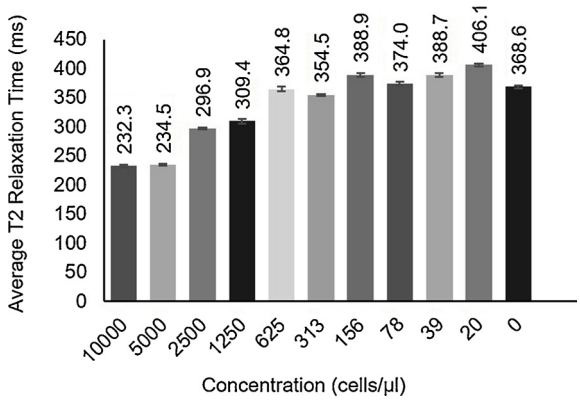

Fig. 3. Magnetic resonance imaging (MRI) of stem cells labeled with Prussian blue nanocubes (PBNCs) *in vitro*. MRI studies were conducted with the same phantom used in the photoacoustic studies. Coronal images were acquired using a multi-slide multi-echo (MSME) sequence to determine average T2 relaxation times. T2 relaxation time increased with decreasing cell concentration.

Feasibility of US/PA imaging as an intraoperative tool to guide needle insertion into the spinal cord was studied prior to direct injection of PBNC-labeled MSCs (Fig. 4). US/PA images were acquired in real-time as the needle was advanced into the spinal cord of Sprague-Dawley rats *ex vivo* (Supplementary video 1). Ultrasound (grayscale) imaging provided anatomical context for needle placement (Fig. 4), but the 33 G needle shaft was difficult to detect (Fig. 4A – D). However, the needle was easily visualized with PA imaging (colorscale) (Fig. 4E – H).

Real-time US/PA images were acquired throughout a 4 μl injection of PBNC-labeled MSCs (Fig. 5, Supplementary video 2). Images were segmented so that the needle shaft primarily appeared blue and PBNC-labeled MSCs appeared red. During the injection, PBNC-labeled MSCs suspended at 10k cells/μl, a clinically relevant cell concentration, were detected when at least 1 μl of solution was injected (Fig. 5B). The average PA signal increased as a function of injection volume (Fig. 5E). Results provided proof-of-concept that PA imaging augmented with PBNCs can provide real-time feedback on MSC delivery.

PBNCs simultaneously possess optical and magnetic properties. Thus, our imaging approach can extend to postoperative MRI. The spinal cord was injected with approximately 2 μl or 5 μl of PBNC-

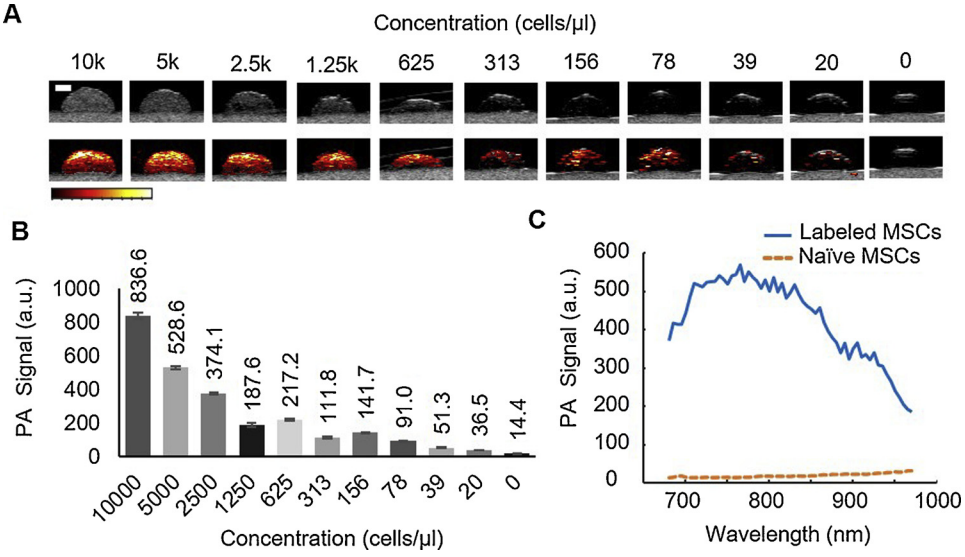

Fig. 2. Photoacoustic (PA) signal of stem cells labeled with PBNCs *in vitro*. Mesenchymal stem cells (MSCs) were incubated with Prussian blue nanocubes (PBNCs) at a concentration of 1 optical density (OD) in culture. PBNC-labeled stem cells were collected and suspended in a tissue-mimicking gelatin phantom with inclusions to analyze the PA signal according to cell concentration. Each dome-shaped inclusion contains PBNC-labeled MSCs (A). Top row: ultrasound (grayscale) images of inclusions. Bottom row: combined ultrasound (grayscale) and photoacoustic (colorscale) images. (B) Average PA signal decreased with cell concentration. (C) Representative PA spectrum of PBNC-labeled MSCs at 5k cells/μl. Scale bar = 2 mm.

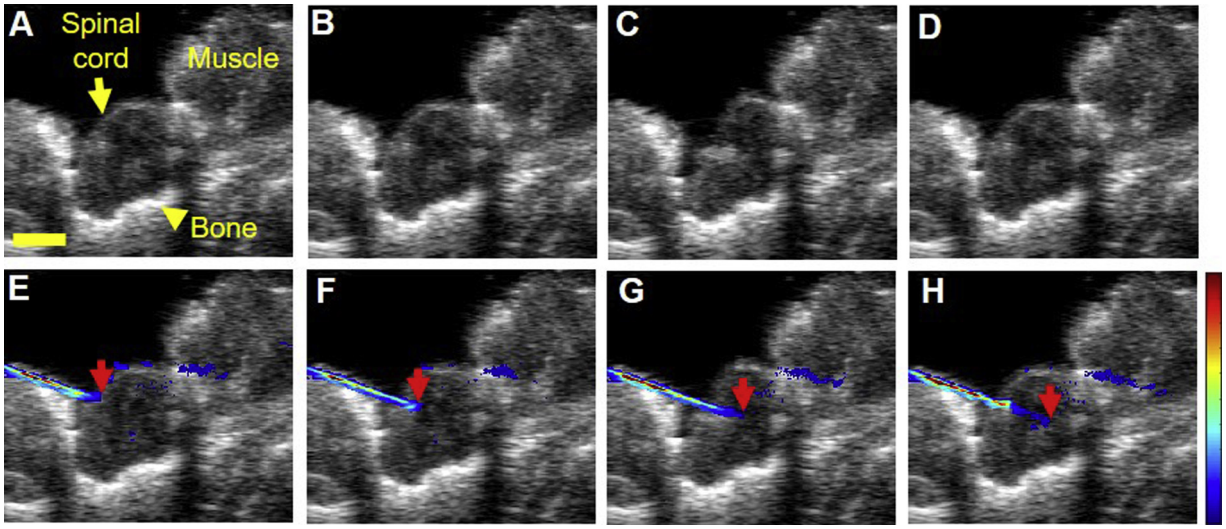

Fig. 4. Ultrasound and photoacoustic image guidance of needle insertion in a rat spinal cord *ex vivo*. Top row: ultrasound (grayscale) images of spinal cord and surrounding tissue. Bottom row: combined ultrasound (grayscale) and photoacoustic (colorscale) images. Both rows of images are from the same dataset. The needle was difficult to detect with ultrasound only (A - D). Photoacoustic imaging at 740 nm wavelength distinguished a 33 G needle as it was inserted into the tissue in real-time (E – H). Red arrows indicate the needle tip. Scale bar = 2 mm.

labeled MSCs at two locations. US/PA images were acquired first and post-processed to distinguish PA signals from the background and PBNC-labeled MSCs (Fig. 6A – C). Next, a layer of muscle was placed on top of the spinal cord to simulate the transition from intraoperative to postoperative imaging, and MR images were acquired. PBNC-labeled MSCs showed negative contrast in T2- (Fig. 6D – F) and T2*-weighted (Fig. 6G – I) MR images. Injections were observed at similar locations in US/PA and MR images for the 2 µl (Fig. 6B – H) and 5 µl (Fig. 6C – I) injections.

Sagittal US/PA/MR images of the spinal cord were also compared (Fig. 7), allowing visualization of the 2 µl and 5 µl injections in the same imaging frame. US/PA images were acquired without (Fig. 7A) and with (Fig. 7B) a layer of muscle on top of the spinal cord to simulate intraoperative and postoperative imaging, respectively. Both PBNC-labeled MSC injections were detected with PA imaging without and with the additional layer of muscle. MRI confirmed PA results and both injections were detected at similar locations (Fig. 7C). Bright-field photomicrographs further confirmed injection locations for PA/MRI (Fig. 7D, E) and also verified MSCs were still labeled with PBNCs, indicated by blue pigment speckles co-localized with pink cytoplasm (Fig. 7F).

4. Discussion

In the current study, we demonstrated several features supporting intra- and postoperative feasibility of US/PA/MR detection of PBNC-labeled stem cells in the spinal cord, including real-time visualization of the needle and injection guidance, immediate feedback on stem cell delivery, and multimodal stem cell detection. The multimodal contrast of PBNCs was a key factor motivating development of our combined US/PA/MRI approach. Optical absorption of PBNCs provides a new tool for stem cell tracking in the spinal cord using US/PA imaging, which has advantages of real-time feedback, intraoperative compatibility, high contrast and sensitivity, and low cost. Magnetic properties of PBNCs allow simultaneous stem cell detection with MRI, the current gold standard for spinal cord imaging, which may improve translation by maintaining compatibility with a familiar, clinical tool while PA imaging becomes more established in clinic. In our previous work, we

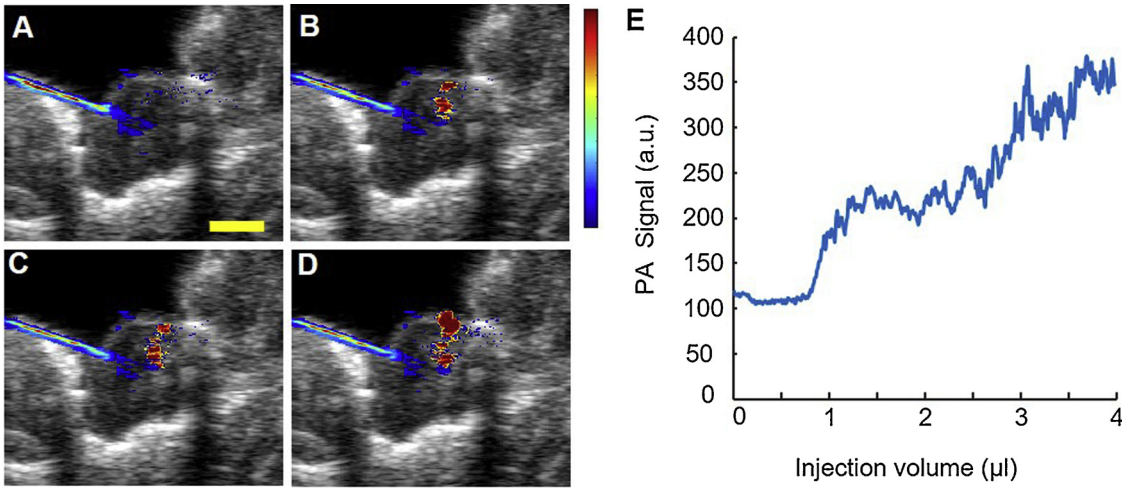

Fig. 5. Injection of PBNC-labeled stem cells in a rat spinal cord *ex vivo*. Throughout the injection, combined ultrasound (grayscale) and photoacoustic (colorscale) images were acquired using a 20 MHz transducer and pulsed laser operating at 740 nm wavelength. (A – D) Images from 0, 1, 2, and 4 µl injected, respectively, at a concentration of 10k cells/µl. (E) Photoacoustic signal increased with injection volume. Scale bar = 2 mm.

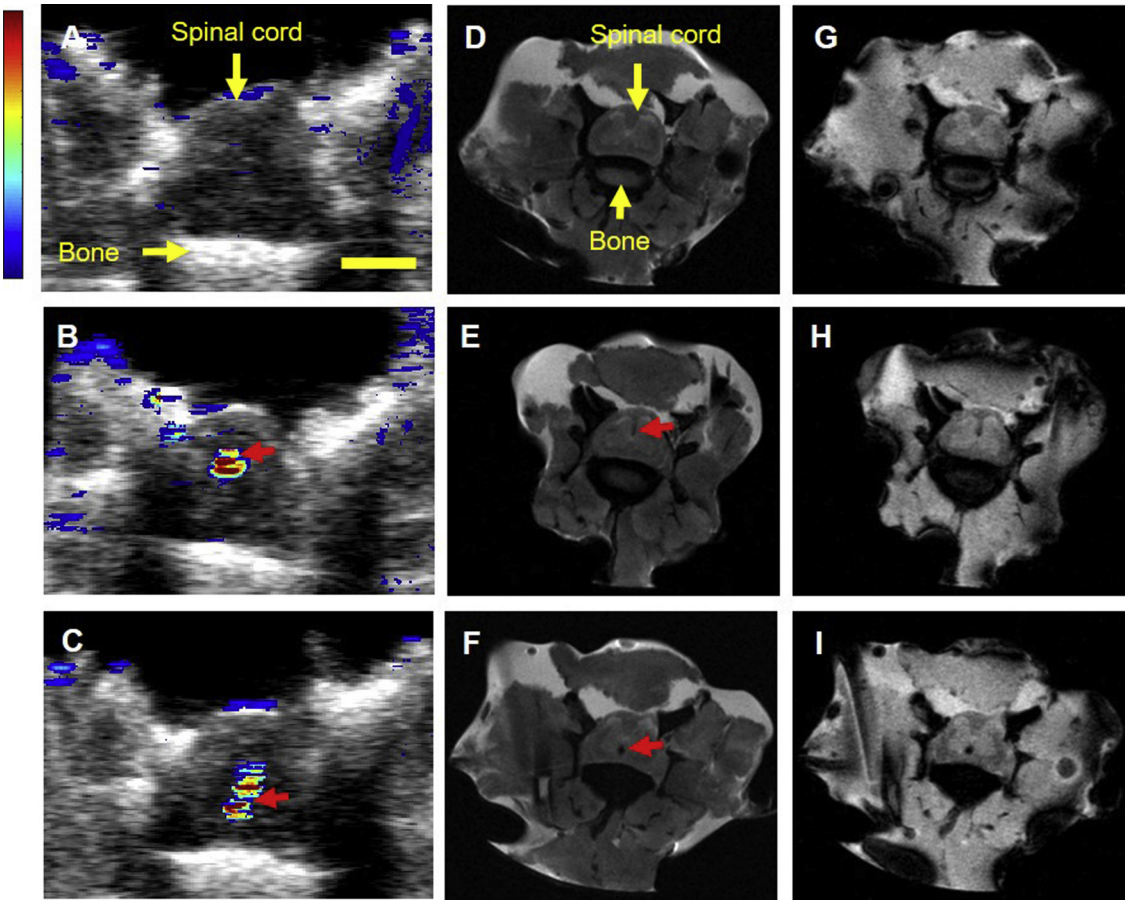

Fig. 6. Multimodal detection of PBNC-labeled stem cells. Prussian blue nanocubes (PBNCs) possess optical and magnetic properties to produce both photoacoustic and magnetic resonance (MR) contrast. PBNC-labeled stem cells were suspended at a concentration of 10k cells/μl. Top row: control, no cells injected. Middle row: 2 μl injection of PBNC-labeled stem cells. Bottom row: 5 μl injection of PBNC-labeled stem cells. Photoacoustic images (A - C) were acquired at 740 nm wavelength. Muscle was placed over the cord prior to MR imaging to simulate the clinical procedure and postoperative imaging protocol. MR images were acquired using T2 (D - F) and T2* (G - I) pulse sequences. Red arrows indicate location of stem cells. Scale bar = 2 mm.

explored the use of AuNSs to detect stem cells in the spinal cord using US/PA imaging only; [6] however complimentary information provided by US/PA/MRI augmented with PBNCs can expand stem cell tracking abilities in intra- and postoperative settings for researchers and clinicians.

PBNCs have several advantages compared to other PA contrast agents used for stem cell tracking. Regarding optical properties, PBNCs have a peak optical absorption at longer wavelengths compared to AuNSs, which may improve PA imaging depth and detection [30,36]. The peak optical absorption of gold nanorods (AuNRs) is more similar to that of PBNCs. However, our previous work showed improved photostability of PBNCs compared to bare or silica-coated AuNRs [30,37]. Regarding magnetic properties, PBNCs have the unique ability to produce MR contrast, which is not possible with pure AuNSs or AuNRs. Magnetic contrast may expedite translation due to established clinical use of MRI for spinal cord imaging. Although PBNCs are in preclinical development, precursor components are FDA approved, which may further simplify regulatory hurdles and translation. In our previous work, PBNCs showed no effect on stem cell potency or viability, even when they were exposed to higher concentrations of PBNCs than those used here [38]. Long-term cytocompatibility of PBNCs needs to be assessed, but short term results were encouraging and highlight another advantage compared to AuNRs, which have shown cytotoxicity in some reports [39]. For these reasons, PBNCs are an excellent contrast agent choice for stem cell imaging in the spinal cord with clear benefits compared to existing technologies.

We initially compared PA and MRI detection capabilities of PBNC-labeled MSCs *in vitro* using the same tissue-mimicking phantom. Results indicated PA imaging and MRI had a limit of detection on the order of 100 or 1000 cells/ μl, respectively. In addition, a more consistent trend was observed in the PA results (Fig. 2) compared to the MR results (Fig. 3), which can be explained by several reasons. First, similar to the widely used SPIONs, PBNC-labeled MSCs produce negative contrast, which makes quantification with MRI challenging because signal loss may result from factors other than the contrast agent. Second, at high cell concentrations, the MR signal may be saturated. Lastly, orientation and width of the MR image slice relative to the region of interest will impact signal. This is particularly challenging when analyzing a small inclusion of only 40 μl at lower cell concentrations. It is important to recognize that the inclusion volume in the tissue-mimicking phantom was 8 times greater than what will be injected *in vivo*. Overall *in vitro* results indicated PA imaging was more sensitive to PBNC-labeled MSCs and may be the better option for quantitative feedback, but PA and MRI detection capabilities will vary in tissue. More specifically, light penetration will reduce detection capabilities of PA imaging *in vivo*, and MRI may become more favorable. Although it is important to anticipate challenges when moving towards *in vivo* studies, at least 10k cells/μl would be injected, which is over a 10- or 100-fold increase over the MR and PA limits of detection observed here. Furthermore, results indicated feasibility of detection in spinal cord tissue with both PA and MRI using clinically representative parameters.

Features of the US/PA/MR imaging platform augmented with PBNCs were demonstrated in experiments simulating intra- and postoperative situations. PA imaging is inherently well-suited for

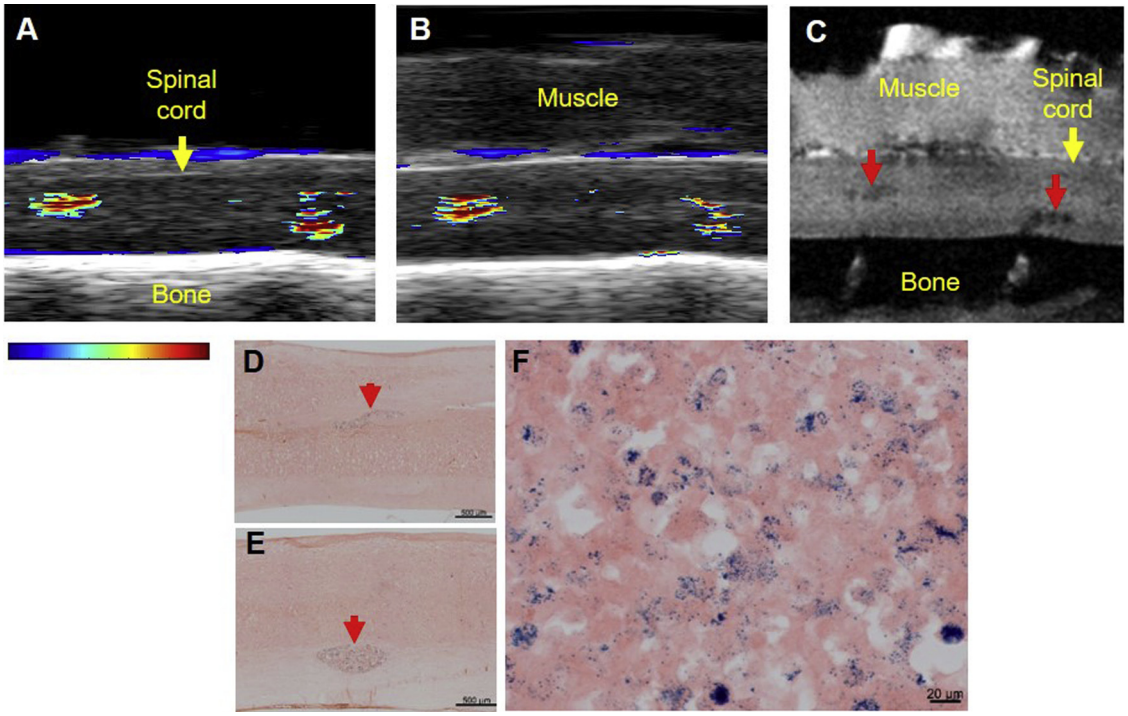

Fig. 7. Multimodal detection of Prussian blue nanocube (PBNC)-labeled stem cells with muscle placed over the spinal cord. PBNC-labeled stem cells suspended at 10k cells/μl were injected twice along the spinal cord, approximately 6 mm apart. Sagittal ultrasound/photoacoustic (A, B) and magnetic resonance (MR) images (C) were acquired. Photoacoustic signals from blood were observed along the top of the cord. Photoacoustic imaging detected the 2 μl (left) and 5 μl (right) injections of PBNC-labeled stem cells before (A) and after (B) a layer of muscle was placed over the spinal cord. The layer of muscle remained on top of the cord for MRI. (C) T2*-weighted MR image. Using MRI, PBNC-labeled stem cells were detected in similar locations as in US/PA images (B). Tissue sections were stained with eosin to confirm results using bright-field microscopy at 10x (D, E) and 40x (F) magnification. Stem cells were co-localized with PBNCs, indicated by blue coloration from the particles (D – F). Red arrows indicate stem cells.

intraoperative imaging due to the smaller foot print, portability, operating room compatibility, lower cost, and fast image acquisition to allow real-time guidance. Although intraoperative MRI exists, implementation is challenging and high cost may be limiting [14–16]. One feature of intraoperative US/PA imaging was guidance of the direct stem cell injection into the spinal cord in intraoperative-mimicking scenarios. Research has shown that direct injection into the spinal cord has higher likelihood of therapeutic success [35]. However, it comes with a higher risk as damage to the spinal cord is more likely. Intraoperative needle guidance can help assure safe needle placement and success of the stem cell injection [3,40].

We previously showed the use of ultrasound only to guide needle placement into the spinal cord [6]. In the current study, the needle shaft was barely visible using ultrasound alone, but was clearly visible with PA imaging. One reason for this is the angular dependence of ultrasound [41]. Compared to ultrasound, PA imaging is less dependent on the object angle relative to the transducer because contrast is based on light absorption, not backscattering. As a result strong PA signals can be more easily generated from the needle shaft regardless of orientation [41]. In addition, because the current US/PA system uses unfocused light delivery, a strong absorber like a metallic needle may be able to absorb enough out of plane light to produce a PA signal. This also simplifies PA image-guidance because the transducer does not need to be perfectly aligned with the needle shaft for PA visualization. For these reasons, intraoperative PA imaging may be a better option for needle guidance due to easier alignment of the transducer and needle shaft. However, intraoperative ultrasound image-guidance will still play a role, as it provides critical anatomical context.

After needle placement, the PBNC-labeled MSC injection was detected in real-time with US/PA imaging. From a clinical perspective, results can provide physicians with immediate, intraoperative feedback on injection success. Currently, delivery success would likely be confirmed with postoperative MRI as intraoperative systems are not commonly available in all clinics. Thus, if stem cell delivery failed, another surgery may be required, highlighting another benefit of the intraoperative US/PA imaging approach. In a research setting, therapy development can also proceed more efficiently by immediately confirming delivery success. US/PA images of the spinal cord acquired during the intraoperative-mimicking scenario were compared to MRI. There was good agreement between modalities, and PBNC-labeled MSCs were detected at similar locations. Some differences in the injection footprint were observed and were suspected to result from differences in imaging slice and sensitivity of PA and MRI to PBNCs.

To assess postoperative potential of the US/PA/MRI approach, a layer of muscle was replaced on top of the spinal cord post-injection to simulate the clinical procedure. Even in clinic, bone is not replaced after the surgery, [33] providing a US/PA imaging window, but MRI still has the advantage for imaging PBNC-labeled MSCs in postoperative scenarios due to greater imaging depth. However, PBNC-labeled MSCs were still detectable with PA imaging in spite of the additional muscle layer, indicating postoperative US/PA imaging may be feasible in small animals in the immediate future. Although additional challenges are expected *in vivo*, including blood and tissue swelling post-surgery which will increase the required imaging depth, comparable stem cell detection between PA and MRI in this simplified model is an important step to support further development of PA imaging in the spinal cord using PBNCs.

Several factors must be considered for translation of the imaging approach to large animal models or humans. Translation of intraoperative US/PA or postoperative ultrasound to large animal models or humans is feasible due to lack of bone to create a convenient imaging window. However, postoperative PA imaging will be limited by light penetration. Technological advances using longer wavelengths, tomographic PA systems, or embedded light sources and light delivery

systems could eventually allow postoperative PA imaging of stem cell therapies in the spinal cord of large animals or humans. In the meantime, MRI can provide sufficient depth for postoperative detection of PBNC-labeled stem cells in clinic immediately.

5. Conclusions

Results showed proof-of-concept of a US/PA/MR imaging approach to guide injection and detect stem cell delivery in the spinal cord. A key aspect of this approach is the use of a unique formulation of Prussian blue nanocubes to produce multimodal PA/MR contrast. MSCs were labeled with 200 nm PBNCs in culture. *Ex vivo* US/PA/MRI studies in rats demonstrated several features supporting intra- and postoperative usability, including real-time needle and injection guidance, immediate feedback on stem cell delivery success, and multimodal stem cell detection. PA and MR images showed good agreement on stem cell location in intra- and postoperative scenarios. Overall PBNCs may facilitate new opportunities to guide stem cell therapies in the spinal cord, and results lay the groundwork for a customizable imaging approach.

Funding

This work was supported in part by the grants from the National Institutes of Health (EB015007 and EY030071).

Declaration of Competing Interest

The authors declare that there are no conflicts of interest.

Acknowledgments

MRI studies were performed at the Magnetic Resonance Imaging Core at the Parker H. Petit Institute for Bioengineering and Bioscience at the Georgia Institute of Technology. The authors wish to thank Dr. Johannes Leisen for sharing his expertise and assisting with MRI studies.

Bright-field microscopy was performed at the Optical Microscopy Core at the Parker H. Petit Institute for Bioengineering and Bioscience at the Georgia Institute of Technology.

This work was performed in part at Georgia Tech's Institute for Electronics and Nanotechnology, a member of the National Nanotechnology Coordinated Infrastructure, which is supported by the National Science Foundation (grant no. ECCS-1542174).

Appendix A. Supplementary data

Supplementary material related to this article can be found, in the online version, at doi:https://doi.org/10.1016/j.pacs.2020.100166.

References

[1] O. Lindvall, Z. Kokaia, A. Martinez-Serrano, Stem cell therapy for human neurodegenerative disorders–how to make it work, Nat. Med. 10 (2004) S42–S50, https://doi.org/10.1038/nm1064.
[2] O. Lindvall, Z. Kokaia, Stem cells in human neurodegenerative disorders - time for clinical translation? J. Clin. Invest. 120 (2010) 29–40, https://doi.org/10.1172/JCI40543.
[3] E.M. Donnelly, J. Lamanna, N.M. Boulis, Stem cell therapy for the spinal cord, Stem Cell Res. Ther. 3 (2012) 24, https://doi.org/10.1186/scrt115.
[4] N.M. Boulis, T. Federici, J.D. Glass, J.S. Lunn, S.A. Sakowski, E.L. Feldman, Translational stem cell therapy for amyotrophic lateral sclerosis, Nat. Rev. Neurol. 8 (2012) 172–176, https://doi.org/10.1038/nrneurol.2011.191.
[5] J.S. Lunn, S.A. Sakowski, T. Federici, J.D. Glass, N.M. Boulis, E.L. Feldman, Stem cell technology for the study and treatment of motor neuron diseases, Regen. Med. 6 (2011) 201–213, https://doi.org/10.2217/rme.11.6.
[6] E.M. Donnelly, K.P. Kubelick, D.S. Dumani, S.Y. Emelianov, Photoacoustic Image-Guided Delivery of Plasmonic-Nanoparticle-Labeled Mesenchymal Stem Cells to the Spinal Cord, Nano Lett. 18 (2018) 6625–6632, https://doi.org/10.1021/acs.nanolett.8b03305.
[7] J.J. Lamanna, J.H. Miller, J.P. Riley, C.V. Hurtig, N.M. Boulis, Cellular therapeutics delivery to the spinal cord: technical considerations for clinical application, Ther. Deliv. 4 (2013) 1397–1410, https://doi.org/10.4155/tde.13.111.
[8] S.Y. Nam, L.M. Ricles, L.J. Suggs, S.Y. Emelianov, Imaging strategies for tissue engineering applications, Tissue Eng. Part B Rev. 21 (2014) 1–44, https://doi.org/10.1089/ten.TEB.2014.0180.
[9] J.J. Lamanna, L.N. Urquia, C.V. Hurtig, J. Gutierrez, C. Anderson, P. Piferi, T. Federici, J.N. Oshinski, N.M. Boulis, Magnetic resonance imaging-guided transplantation of neural stem cells into the porcine spinal cord, Stereotact. Funct. Neurosurg. 95 (2017) 60–68, https://doi.org/10.1159/000448765.
[10] J.J. Lamanna, J. Gutierrez, L.N. Urquia, C.V. Hurtig, E. Amador, N. Grin, C.N. Svendsen, T. Federici, J.N. Oshinski, N.M. Boulis, Ferumoxytol labeling of human neural progenitor cells for diagnostic cellular tracking in the porcine spinal cord with magnetic resonance imaging, Stem Cells Transl. Med. 6 (2017) 139–150, https://doi.org/10.5966/sctm.2015-0422.
[11] A. Chotivichit, M. Ruangchainikom, P. Chiewvit, A. Wongkajornsilp, K. Sujirattanawimol, Chronic spinal cord injury treated with transplanted autologous bone marrow-derived mesenchymal stem cells tracked by magnetic resonance imaging: a case report, J. Med. Case Rep. 9 (2015) 79, https://doi.org/10.1186/s13256-015-0535-6.
[12] E. Syková, P. Jendelová, Magnetic resonance tracking of transplanted stem cells in rat brain and spinal cord, Neurodegener. Dis. 3 (2006) 62–67, https://doi.org/10.1159/000092095.
[13] F. Callera, C.M.T.P. de Melo, Magnetic resonance tracking of magnetically labeled autologous bone marrow CD34 + cells transplanted into the spinal cord via lumbar puncture technique in patients with chronic spinal cord injury: CD34 + cells' migration into the injured site, Stem Cells Dev. 16 (2007) 461–466, https://doi.org/10.1089/scd.2007.0083.
[14] D. Netuka, S. Ostry, T. Belsan, F. Kramar, V. Benes, Intraoperative MR imaging in a case of a cervical spinal cord lesion, J. Neurosurg. Spine 14 (2011) 754–757, https://doi.org/10.3171/2011.2.SPINE10715.
[15] T.P. Duprez, A. Jankovski, C. Grandin, L. Hermoye, G. Cosnard, C. Raftopoulos, Intraoperative 3T MR imaging for spinal cord tumor resection: feasibility, timing, and image quality using a "Twin" MR-Operating suite, Am. J. Neuroradiol. 20 (2008) 1547–1553, https://doi.org/10.3174/ajnr.a1134.
[16] F.A. Jolesz, A.J. Golby, D.A. Orringer, Magnetic resonance image-guided neurosurgery, Intraoperative Imaging Image-Guided Ther, Springer, New York, 2014, pp. 451–463, https://doi.org/10.1007/978-1-4614-7657-3_32.
[17] G.P. Luke, D. Yeager, S.Y. Emelianov, Biomedical applications of photoacoustic imaging with exogenous contrast agents, Ann. Biomed. Eng. 40 (2012) 422–437, https://doi.org/10.1007/s10439-011-0449-4.
[18] P. Beard, Biomedical photoacoustic imaging, Interface Focus 1 (2011) 602–631, https://doi.org/10.1098/rsfs.2011.0028.
[19] M. Xu, L.V. Wang, Photoacoustic imaging in biomedicine, Cit. Rev. Sci. Instruments J. Appl. Phys. 77 (2006) 41101–102027, https://doi.org/10.1063/1.2195024.
[20] L.V. Wang, S. Hu, Photoacoustic tomography: in vivo imaging from organelles to organs, Science (80-.) 335 (2012) 1458–1462, https://doi.org/10.1126/science.1216210.
[21] S.Y. Emelianov, P.-C. Li, M. O'Donnell, Photoacoustics for molecular imaging and therapy, Phys. Today 62 (2009) 34–39.
[22] J. Weber, P.C. Beard, S.E. Bohndiek, Contrast agents for molecular photoacoustic imaging, Nat. Methods 13 (2016) 639–650, https://doi.org/10.1038/nmeth.3929.
[23] T. Kim, J.E. Lemaster, F. Chen, J. Li, J.V. Jokerst, Photoacoustic imaging of human mesenchymal stem cells labeled with Prussian blue?poly (l-lysine) nanocomplexes, ACS nano 11 (9) (2017) 9022–9032.
[24] L. Cheng, H. Gong, W. Zhu, J. Liu, X. Wang, G. Liu, Z. Liu, PEGylated Prussian blue nanocubes as a theranostic agent for simultaneous cancer imaging and photothermal therapy, Biomaterials. 35 (2014) 9844–9852, https://doi.org/10.1016/j.biomaterials.2014.09.004.
[25] Z. Li, Y. Zeng, D. Zhang, M. Wu, L. Wu, A. Huang, H. Yang, X. Liu, J. Liu, Glypican-3 antibody functionalized Prussian blue nanoparticles for targeted MR imaging and photothermal therapy of hepatocellular carcinoma, J. Mater. Chem. B. 2 (2014) 3686–3696, https://doi.org/10.1039/c4tb00516c.
[26] G. Fu, W. Liu, Y. Li, Y. Jin, L. Jiang, X. Liang, S. Feng, Z. Dai, Magnetic prussian blue nanoparticles for targeted photothermal therapy under magnetic resonance imaging guidance, Bioconjug. Chem. 25 (2014) 1655–1663, https://doi.org/10.1021/bc500279w.
[27] L. Jing, X. Liang, Z. Deng, S. Feng, X. Li, M. Huang, C. Li, Z. Dai, Prussian blue coated gold nanoparticles for simultaneous photoacoustic/CT bimodal imaging and photothermal ablation of cancer, Biomaterials 35 (2014) 5814–5821, https://doi.org/10.1016/j.biomaterials.2014.04.005.
[28] X. Liang, Z. Deng, L. Jing, X. Li, Z. Dai, C. Li, M. Huang, Prussian blue nanoparticles operate as a contrast agent for enhanced photoacoustic imaging, Chem. Commun. 49 (2013) 11029–11031, https://doi.org/10.1039/c3cc42510j.
[29] M. Shokouhimehr, E.S. Soehnlen, A. Khitrin, S. Basu, S.D. Huang, Biocompatible Prussian blue nanoparticles: preparation, stability, cytotoxicity, and potential use as an MRI contrast agent, Inorg. Chem. Commun. 13 (2010) 58–61, https://doi.org/10.1016/j.inoche.2009.10.015.
[30] D.S. Dumani, J.R. Cook, K.P. Kubelick, J.J. Luci, S.Y. Emelianov, Photomagnetic Prussian blue nanocubes: synthesis, characterization, and biomedical applications, Nanomed. Nanotechnol. Biol. Med. (2019) 102138, https://doi.org/10.1016/j.nano.2019.102138.
[31] J.R. Cook, R.R. Bouchard, S.Y. Emelianov, Tissue-mimicking phantoms for photoacoustic and ultrasonic imaging, Biomed. Opt. Express 2 (2011) 3193, https://doi.org/10.1364/BOE.2.003193.
[32] D.A. Armbruster, T. Pry, Limit of blank, limit of detection and limit of quantitation, Clin. Biochem. Rev. 29 (Suppl 1) (2008) S49–S52.

[33] J.D. Glass, N.M. Boulis, K. Johe, S.B. Rutkove, T. Federici, M. Polak, C. Kelly, E.L. Feldman, Lumbar intraspinal injection of neural stem cells in patients with amyotrophic lateral sclerosis: results of a phase I trial in 12 patients, Stem Cells 30 (2012) 1144–1151, https://doi.org/10.1002/stem.1079.
[34] B. Raore, T. Federici, J. Taub, M.C. Wu, J. Riley, C.K. Franz, M.A. Kliem, B. Snyder, E.L. Feldman, K. Johe, N.M. Boulis, Cervical multilevel intraspinal stem cell therapy: assessment of surgical risks in Gottingen Minipigs, Spine 36 (3) (2011) E164–E171.
[35] C. Paul, A.F. Samdani, R.R. Betz, I. Fischer, B. Neuhuber, Grafting of human bone marrow stromal cells into spinal cord injury: a comparison of delivery methods, Spine 34 (2009) 328–334, https://doi.org/10.1097/BRS.0b013e31819403ce.
[36] S.Y. Nam, L.M. Ricles, L.J. Suggs, S.Y. Emelianov, Nonlinear photoacoustic signal increase from endocytosis of gold nanoparticles, Opt. Lett. 37 (2012) 4708–4710.
[37] Y.-S. Chen, W. Frey, S. Kim, K. Homan, P. Kruizinga, K. Sokolov, S. Emelianov, Enhanced thermal stability of silica-coated gold nanorods for photoacoustic imaging and image-guided therapy, Opt. Express 18 (2010) 8867, https://doi.org/10.1364/OE.18.008867.
[38] E.J. Snider, K.P. Kubelick, K. Tweed, R.K. Kim, Y. Li, K. Gao, A.T. Read, S. Emelianov, C.R. Ethier, Improving stem cell delivery to the trabecular meshwork using magnetic nanoparticles, Sci. Rep. 8 (2018) 12251, https://doi.org/10.1038/s41598-018-30834-7.
[39] A.M. Alkilany, P.K. Nagaria, C.R. Hexel, T.J. Shaw, C.J. Murphy, M.D. Wyatt, Cellular uptake and cytotoxicity of gold nanorods: molecular origin of cytotoxicity and surface effects, Small 5 (2009) 701–708, https://doi.org/10.1002/smll.200801546.
[40] J. Riley, J. Butler, K.B. Baker, S. McClelland III, Q. Teng, J. Yang, M. Garrity-Moses, T. Federici, N.M. Boulis, Targeted spinal cord therapeutics delivery: stabilized platform and microelectrode recording guidance validation, Stereotact. Funct. Neurosurg. 86 (2008) 67–74, https://doi.org/10.1159/000112426.
[41] J. Su, A. Karpiouk, B. Wang, S. Emelianov, Photoacoustic imaging of clinical metal needles in tissue, J. Biomed. Opt. 15 (2010) 021309, , https://doi.org/10.1117/1.3368686.

Kelsey P. Kubelick Kelsey Kubelick is in the Wallace H. Coulter Department of Biomedical Engineering and the School of Electrical and Computer Engineering at the Georgia Institute of Technology and Emory University. Her research focuses on development of cell and particle tracking approaches using ultrasound, photoacoustic, and magnetic resonance imaging to expedite translation of novel therapies, particularly in the fields of regenerative medicine and immunology.

Stanislav Emelianov Dr. Stanislav Emelianov is a Joseph M. Pettit Endowed Chair, Georgia Research Alliance Eminent Scholar, and Professor of Electrical & Computer Engineering and Biomedical Engineering at the Georgia Institute of Technology and Emory University School of Medicine. Furthermore, Dr. Emelianov is Director of the Ultrasound Imaging and Therapeutics Research Laboratory. Projects in Dr. Emelianov's laboratory are focused on the discovery, development, and clinical translation of diagnostic imaging and therapeutic instrumentation, augmented with theranostic nanoagents.